Sensors and Actuators B 237 (2016) 841–848

Contents lists available at ScienceDirect

Sensors and Actuators B: Chemical

journal homepage: www.elsevier.com/locate/snb

High-throughput on-line multi-detection for refractive index, velocity, size, and concentration measurements of micro-two-phase flow using optical microfibers

Yu-Wen Hsieh [a], An-Bang Wang [a,*], Xuan-Yi Lu [b], Lon A. Wang [b,c]

[a] Institute of Applied Mechanics, National Taiwan University, No.1, Sec.4, Roosevelt Rd., Taipei 10617, Taiwan
[b] Graduate Institute of Photonics and Optoelectronics, National Taiwan University, No.1, Sec.4, Roosevelt Rd., Taipei 10617, Taiwan
[c] Department of Electrical Engineering, National Taiwan University, No.1, Sec.4, Roosevelt Rd., Taipei 10617, Taiwan

ARTICLE INFO

Article history:
Received 9 May 2016
Received in revised form 27 June 2016
Accepted 6 July 2016
Available online 7 July 2016

Keywords:
On-line measurement
High-throughput
Multi-detection
Micro-two-phase flow
Optical microfiber

ABSTRACT

We demonstrate that high-throughput on-line multi-detection (refractive index, segment velocity, size, and concentration) with high resolution can be achieved simultaneously for micro-two-phase flow by microfibers in the microfluidic chip. The microfibers were immersed in the fluid channel in perpendicular to the flow direction with direct contact of test samples to increase the space resolution and detection sensitivity. A novel "soft sealing" method has been developed for microfiber installing in microfluidic chip, where the continuous phase fluid is applied to surround the microfiber and protect it from vibrations and chip-wall contact, to stabilize the microfiber signal. The time-domain microfiber signal is directly applied to quantify the refractive index of test samples, and different operation modes of this measuring technique have been systematically analyzed. With only tiny sample volume (~100 nanoliters), the measurement resolution for refractive index and concentration can reach 2×10^{-4} and 2×10^{-3}, respectively. For both velocity and size measurements, the maximum deviation between this measuring technique and image analysis method is less than 3%, while the overall measurement uncertainty is no more than 3.4%.

1. Introduction

Over the past two decades, bubble/droplet-based microfluidics has drawn surge attentions in applications such as high-throughput screening [1], rapid droplet sorting [2], biochemical micro-reactor [3], functional micro-particle synthesis [4], and even bubble logic [5]. All these progresses do offer a promising potential of bubble/droplet-based microfluidics for wide applications in our future life. However, the on-line measurement for the micro-bubble/droplet generation systems, which is critical for quantitative analyses of segmented flows, has not drawn much attention. Among the sensing techniques used in the literature, bright-field microscopy is the most simple and commonly used tool for monitoring the motions and contours of bubbles/droplets [6–9], but test samples with low contrast are not easily distinguishable in common biochemical analyses by illumination of visible light. Accordingly, high quality images need to be obtained by labelling the specific biochemical compound by using fluorescent reagents with the aid of proper filters [10–13]. Nonetheless, long exposure time is required for the dim light illuminated by fluorescence to enhance the signal-to-noise ratio, which restricts the limit of analysis frequency to be only around 10^1 Hz. The optical absorption technique, where a set of separated optical emitter and receiver used to measure the variation of light absorption caused by different sample concentrations, is frequently utilized in droplet-based microfluidics [14–17]. Although this approach has advantages of lower cost and higher analysis frequency (~10^2 Hz), it has generally lower sensitivity due to the inherently short optical path in microfluidic systems. Precise positioning of the separated optical emitter and receiver is also critical to ensure the system sensitivity and space resolution. This method has been applied to measure the properties of single cells by optical resonator and interference [18,19]. The spectral shift of the cell, which was trapped by delicate controlling two different buffer fluids, was used to quantify the refractive index and size of the cell. No calibration is required to maintain the high precision of measurements; however, the analysis speed is restricted by the buffer change process. Electrochemical detection is another developed technique, in which the dielectricity [20,21] or conductivity [22–24] of working fluids are measured to quantify the size, velocity, or concentration

* Corresponding author.
E-mail address: abwang@spring.iam.ntu.edu.tw (A.-B. Wang).

http://dx.doi.org/10.1016/j.snb.2016.07.027
0925-4005/

of droplets. Its advantages are rapid response (~10^3 Hz) and high sensitivity; nevertheless, the multi-processing micro-fabrication of electrodes inside the microfluidic chip has increased the cost. As to the laser-induced fluorescence method [25–29], the molecules to be examined are excited by laser and then emit light with wavelength different to the excitation one. It has very high sensitivity, analysis frequency (over 10^3 Hz), and space resolution (~10 μm), but labelling of test samples is always necessary that restricts its general usages. By contrast, Raman spectroscopy method detects the sample contents without labelling but by the Raman shift [30–34], which is originated from Raman scattering of specific molecules. This technique could detect multiple molecules simultaneously in a relatively fast and sensitive manner, but the system is the most expensive among others. Although there are a variety of sensing methods for bubble/droplet-based microfluidics, the technique for measuring the refractive index of micro-bubbles/droplets is still scarce up to now.

For the scientific analysis, the refractive index is one of the key properties that determine a material. By introducing the optical evanescent field, Polynkin et al. [35] orthogonally laid an optical microfiber a few microns below the microfluidic channel to measure the refractive index of a single-phase-flow. This method has demonstrated the great potentials of using optical microfiber for high sensitivity, rapid response, and low cost measurement. However, the fabrication process is not easy to be reproducible since the embedding and precision positioning of very fine optical microfibers (~1 μm in diameter) is very difficult. Recently, this technique was modified to be the intrusive type [36–38] for enhancing the signal intensity, and the optical microfiber was aligned in the center of the microchannel along the flow direction to solve the sensor embedding and positioning problems. However, the space resolution becomes low (~10^1 mm) due to the long microfiber contact length in the microfluidic channel. Moreover, to acquire a stable sensing signal, the microfiber has to be fully immerged in the test sample. The sample loading and cleaning processes thus hinder the throughput of detection. This technique has been further improved by constructing optical waveguides along the microfluidic channel through microlithography to enhance the space resolution (~1 mm), and it was applied to measure the segment size of nitrogen–water flow [17]. Again, owing to the long contact length, it is difficult to capture the segment dynamics precisely. In addition, the on-line size measurement for the flow with unstable or unknown flowrate is basically not possible since its size measurement of droplets/bubbles was based on the given and averaged flowrate of syringe pumps or pressure driven systems.

In the present study, to overcome the long-time existing problem of low space resolution for immersed microfiber, the microfluidic chip was designed as a microfluidic channel orthogonally across the optical microfiber sensor(s), as shown in Fig. 1, by using a novel "soft sealing" design but without the need of precision alignment. No clean room, no micro-fabrication process, and no need of spectrometer are proposed to achieve the low cost target of the present work for the wide applications in future. The time-domain signal was utilized to directly acquire the properties of test samples, e.g., the refractive index and sample concentration, and tested for the high-throughput on-line measuring performance. Furthermore, by implementing a pair of optical microfibers in the microfluidic channel, the instantaneous segment size and velocity measurements were also evaluated for both liquid–liquid and gas-liquid two-phase flows.

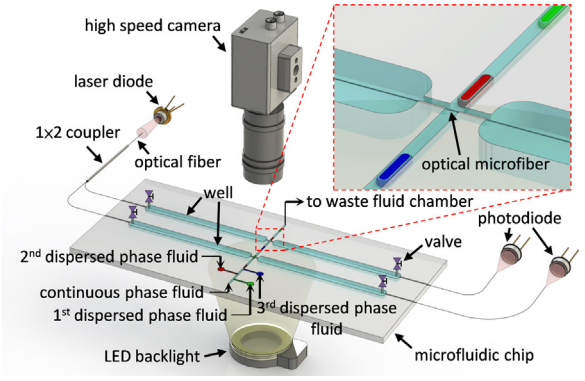

Fig. 1. Experimental setup of the micro-bubble/droplet generator and the optical microfiber detection system. Two optical microfibers were embedded inside the microfluidic chip and were laid 1 cm apart across the main channel.

2. Methods and materials

2.1. Experimental setup of the integrated optical sensing system

It is well-known that the transmission direction and intensity of a light across different materials depend on their relative reflective indexes that the light conducts across, i.e. Snell's law. This means that the light power transmitting through an optical microfiber is highly sensitive to the refractive index of its surrounding medium. Therefore, the refractive index of fluids can be directly measured based on the variations of transmitted light power by immersing the microfiber in different fluids once the optical microfiber system has been calibrated in the given fluids with known refractive indexes.

As shown in Fig. 1, the optical microfibers with refractive index $n_f = 1.45$ were placed in perpendicular to the main microfluidic channel, and they were sealed by using the "soft sealing" design inside the Polymethylmethacrylate (PMMA) microfluidic chip with refractive index $n_{PMMA} = 1.49$. To conduct the "soft sealing" process, the continuous phase fluid with refractive index $n_c < n_f$ was firstly injected into four wells to replace the gas that surrounded the microfiber. The well inlets were then closed by four solenoid valves for keeping the rigidity of "liquid walls". This soft sealing method has three major contributions. First, the test samples were blocked from entering the well, which could automatically prevent the leakage and contamination problems of test fluids. Second, the microfibers were prevented from touching the channel wall, and the leakage of optical power can thus be completely suppressed. Finally, the continuous phase fluid helps to damp the vibration of microfiber as test samples passing through it, which greatly enhances the stability of the sensing signal. With the aid of perfect sealing, stable time-domain signal with high space resolution of detection can thus be easily achieved. To minimize the needed test fluid samples, a T-junction structure with 500 μm in width and 300 μm in height for both main and side channels was applied to generate stable two-phase bubble/droplet flows for measurements. The detailed fabrication processes of the integrated optical microfiber chip are stated in ESI S.1.

A 1550 nm laser diode (LPSC-1550-FC, Thorlabs) with 10 mW optical input power was used for all experiments. The laser light was guided in an optical fiber and separated into two beams by a 1 × 2 (50/50) fiber coupler (F-CPL-F12155- FCAPC, Newport) before immersing in the microfluidic Chip. These two tapered optical microfibers, with 10 μm in diameter in the microfluidic channel and 125 μm in diameter at both ends, could be easily plugged in the predetermined wells with a spacing of 1 cm in the microfluidic chip. High velocity resolution of detection can thus be easily achieved without the need of careful positioning and adjustment of each microfiber with spacing uncertainty less than 0.25%. The laser light intensity of each optical microfiber on the other side of microfluidic chip was detected by an InGaAs photodiode (SM05PD4A, Thorlabs),

transformed into electric signal, recorded by a data acquisition device (USB-6341, National Instruments), and then processed by a self-developed LabVIEW program. The data sampling rate was 20,000 Hz for all tests, i.e., with the time resolution of 50 μs.

It is worth noting that the signal of only one optical microfiber is sufficient for measuring the refractive index of test fluids. The dual-microfiber setup in Fig. 1 was designed for simultaneous velocity and size measurements of micro-bubbles/droplets. Based on this setup, the velocity of fluid segment is derived from the given distance between two microfibers divided by the travelling time measured from two fibers. The segment sizes can be further calculated from the velocity of fluid segment multiplied with the measured passing time of fluid segment through any microfiber. The obtained results by the present microfiber system were compared and validated by the direct visualization method through a high speed camera (FASTCAM Super 10 K, Photron) with a self-developed MATLAB program. A LED ring illuminator with a diffuser was used as the backlight to enhance the image contrast as shown in Fig. 1.

2.2. Working fluids and two-phase flow generation

Distilled water and Hexadecane were used as the continuous phase fluids, and the dispersed phase fluids included air, distilled water, and five glycerol concentrations C_{gly} (30%, 70%, 73%, 80%, and 95% by weight) of glycerol-water solutions. Since most of the biochemistry-related applications are in aqueous solutions and wide range of refractive index can be easily obtained by changing the concentration of glycerol in water, the chemically stable aqueous glycerol solution was then chosen for refractive index calibration of the present microfiber system. To obtain the calibration relationship of the refractive index n and the signal V from the optical microfiber, each working fluid was measured by a refractometer (RA-130, Kyoto Electronics) thrice at 25 °C and averaged. The coefficient of variation of each data was below 0.1%. The maximum refractive index difference of aqueous glycerol solution between the present measurements and that by Hoyt [39] was less than 0.2% (please refer ESI Fig. S2 in detail).

As shown in Fig. 1, the continuous phase fluid (liquid; cyan fluid) and different immiscible dispersed phase fluids (gas or liquid; red, green, and blue fluids) were pumped into the main channel and the side channel. The pumping sources have been chosen as syringe pumps (KDS-210, KD Scientific) or pressure regulators (ER3000, TESCOM). As the two-phase flow passing the optical microfiber, a square-wave-like signal would be detected due to the periodic change of the refractive index of fluid surrounding the microfiber.

3. Results and discussions

3.1. Refractive index measurement

As pure liquid passing around the optical microfiber in the chip, a constant voltage could be obtained from the photodiode. Fig. 2(a) shows the typical DC signal of pure liquids for Hexadecane (green solid line) and distilled water (red solid line) passing the optical microfiber, where V is the instantaneous sensing voltage, and t is the measuring time. On the other hand, a square-wave-like signal (blue solid line in Fig. 2(a)) could be obtained for the two-phase flow, e.g., distilled water droplets in Hexadecane, and the high and low level signals jumped between the above-mentioned two DC-lines. The total flow rate was 6 ml/h for all cases and 3 ml/h of each fluid for the steady two-phase flow case. It shows clearly that the high level and low level voltage of the two-phase flow correspond to the passing of the distilled water and the Hexadecane, respectively. Since distilled water has a smaller refractive

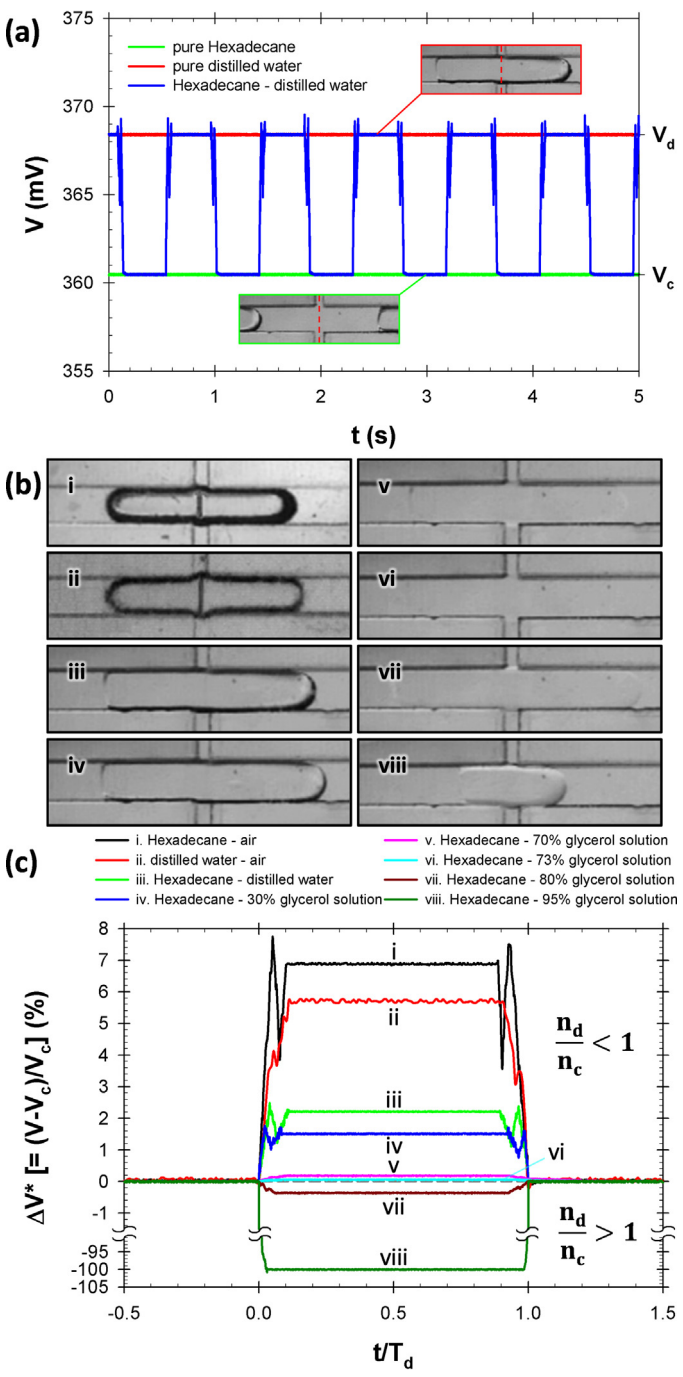

Fig. 2. (a) Typical electric signals of flow passing through the optical microfiber. The red dashed lines in the inset image indicate the location of the optical microfiber. (b) Recorded images of eight combinations of two-phase flows passing through the optical microfiber. (c) Comparison of normalized microfiber signals for different two-phase flows i – viii. (For interpretation of the references to colour in this figure legend, the reader is referred to the web version of this article.)

index than Hexadecane, this creates a favorable environment for the total internal reflection of laser light to transmit inside the optical microfiber based on Snell's law. The photo-sensor thus reflects a high level signal V_d rising from the low level signal V_c as the distilled water droplet of the two-phase flow contacted the microfiber, where the subscript d and c represent the dispersed phase fluid and the continuous phase fluid, respectively. By changing the fluids of the steady two-phase flows, it is observed that the frequency of detected signal is exactly the same as the generation frequency of micro-bubbles/droplets except in the special condition of $n_c = n_d$,

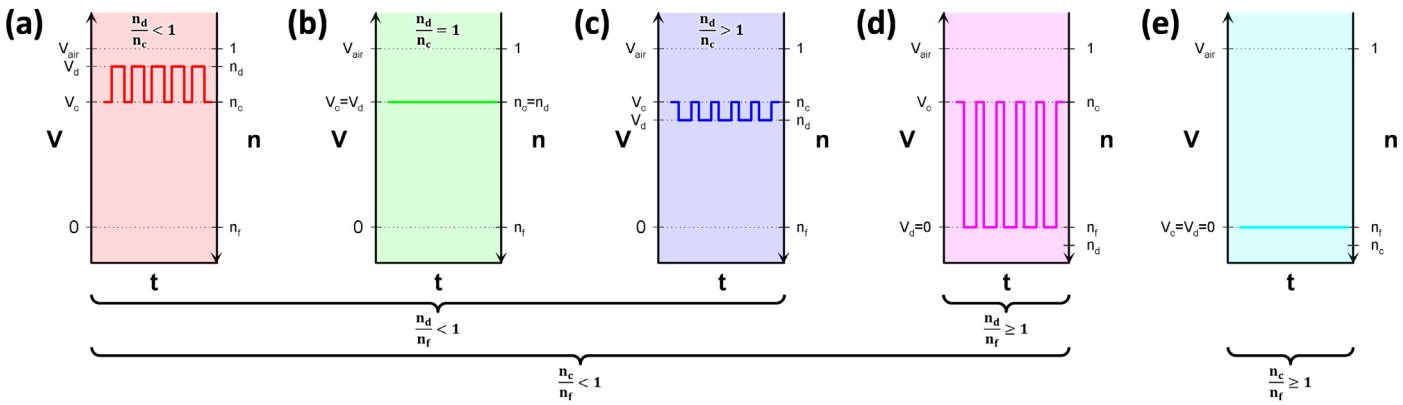

Fig. 3. Classification of microfiber signals V and the corresponding refractive index n of sample fluids under different combinations of n_c, n_d and n_f. (a) $n_d < n_c < n_f$ (b) $n_d = n_c < n_f$ (c) $n_c < n_d < n_f$ (d) $n_c < n_f \leq n_d$ (e) $n_c \geq n_f$.

where no periodic signal can be detected. Moreover, the higher the difference of the refractive index between two fluids is, the larger the measured alternating signal, i.e., $V_d - V_c$, becomes. To simply the description, the two-phase flow is denoted as "A – B flow" thereafter, where the former (A) represents the continuous phase fluid, and the latter (B) is the dispersed phase fluid.

In Fig. 2(b), the images of two-phase flows with eight combinations of different fluids are shown as cases i – viii. All cases have the flow rate 3 ml/h for both continuous phase and dispersed phase fluids except case viii, in which the flow rate of 95% glycerol aqueous solution was only 0.5 ml/h since the high viscosity fluid could not be segmented at higher flow rates. The image contrast of the fluid interfaces reveal how significant the refractive index difference of the continuous phase fluid and the dispersed phase fluid is. The fluid interfaces in cases v and vi are hardly identified by direct observation with general microscope due to too small refractive index difference; however, they could still be clearly measurable by the optical microfiber as shown in Fig. 2(c). To quantitatively compare the microfiber signals of different test cases having various bubble/droplet sizes due to various viscosities of dispersed phase fluids, the dimensionless parameters ΔV^*, defined as $[(V\text{-}V_c)/V_c]$, were used in Fig. 2(c) for fluids of $n_c/n_f < 1$, where T_d is the duration of one dispersed fluid segment passing through the optical microfiber. It shows that the sign of dimensionless dispersed phase fluid signal ΔV_d^* $(=[(V_d\text{-}V_c)/V_c])$ is determined by the ratio of n_d/n_c, i.e., the detected ΔV_d^* is positive for $n_d/n_c < 1$ (here for cases i – vi), negative for $n_d/n_c > 1$ (for cases vii–viii), and zero for $n_d/n_c = 1$. Furthermore, the higher the refractive index difference of the dispersed phase fluid from the continuous phase fluid is, the higher the alternating signal (i.e., absolute value of ΔV_d^*) becomes. It is important to note in case viii that ΔV_d^* drops to −100% as the dispersed phase fluid contacted the optical microfiber and then returned to zero after its passing. This is because the refractive index of 95% aqueous glycerol solution is higher than that of the optical microfiber. The droplet absorbed all laser power from the microfiber during its contact, and thus no laser light was transmitted to the photodiode. This means also that ΔV_d^* remains constant and is n_d-independent for the two phase flow with $n_d \geq n_f > n_c$. As to fluids of $n_c/n_f \geq 1$ (see discussions in ESI S.3), V = 0 was always obtained, i.e., all laser power has been conducted into the continuous phase fluid no matter n_d is higher or lower than n_c. In this situation, the refractive indexes of continuous phase and dispersed phase fluids could not be resolved, and no meaningful signal could be analyzed. Therefore, this is thus not the appropriate working condition for the detection system but can be used as the function of "reset" or "ground."

To summarize the different observations mentioned above, the characteristic relations of sequential output voltage and refractive index combinations of two-phase flows with respect to that of optical microfibers can be classified as shown in Fig. 3. The optical microfiber sensing system proposed in this work should be operated under the condition of $n_c/n_f < 1$ (Fig. 3(a)–(d)) and none output voltage could be detected for $n_c/n_f \geq 1$ (Fig. 3(e)). This means that n_f is the upper bound of the working range of this design, and the operational domain of the system can thus be widened by using high refractive index fibers, e.g., fluoride or tellurite optical fibers. As $n_c/n_f < 1$, both of the refractive indexes of n_d and n_c can be measured for $n_d/n_f < 1$(Fig. 3(a)–(c)), but only n_c can be detected for $n_d/n_f \geq 1$ (Fig. 3(d)). As $n_c/n_f < 1$ and $n_d/n_f < 1$ (Fig. 3(a)–(c)), the signals of V_d and V_c respectively reveal the refractive index of dispersed phase and continuous phase fluids, and the amplitude of the square-wave-like signal represents the refractive index difference between n_c and n_d. These three conditions are suitable for biochemical detection or refractive index matching fluid development. It can also be utilized as Brix meter or salinity meter since the concentration of sugar and salt affects the refractive index of the aqueous solution. For $n_c/n_f < 1$ and $n_d/n_f \geq 1$ (Fig. 3(d)), very high amplitude of square-wave-like signal is obtained since V_d drops to zero. Although the n_d value could not be resolved under this condition, its highly responsive on-off typed signal, where $n_d/n_f = 1$ serves as the threshold, is especially appropriate for sample counting or sorting.

The relationship between ΔV_d^* and Δn, defined as $n_d - n_c$, of cases i – vii is shown in Fig. 4. Each measuring point was averaged from thirty consecutive periods, and the corresponding error bar illustrates the maximum deviations of these thirty measurements. In Fig. 4(a), it shows that ΔV_d^* has a second order polynomial relationship with Δn ($\Delta V_d^* = -16.0\Delta n^2 - 22.6\Delta n$, $R^2 = 0.998$). The logarithmic scale plot of $|\Delta V_d^*|$ versus $|\Delta n|$ is further illustrated in Fig. 4(b). It reveals that, from the present experimental results, the reading of refractive index (i.e., Δn) of this new sensing system has already reached around 10^{-3} in case vi. The base signal (V_c) for microfiber immersed in Hexadecane was about 350 mV with around 0.05 mV peak-to-peak noise. By taking the peak-to-peak amplitude of the noise as the minimum resolved signal for V_d^* in this system, the refractive index resolution is estimated to be 2×10^{-4} from the calibration curve in Fig. 4(b). The corresponding sensitivity of refractive index measurement is 4.48 V^{-1}.

With the calibrated relationship in Fig. 4(b), the n_d of any fluid (with $n_d < n_f$) transported by a continuous phase fluid of known n_c can be easily determined by real-time sensing ΔV_d^* from the present optical microfiber system. This means that the instantaneous small variation of fluid's refractive index caused by biochemical reactions can be also directly and easily on-line monitored or detected by this sensitive method. It is noted that the refractive index of test samples can also be measured by gravity-

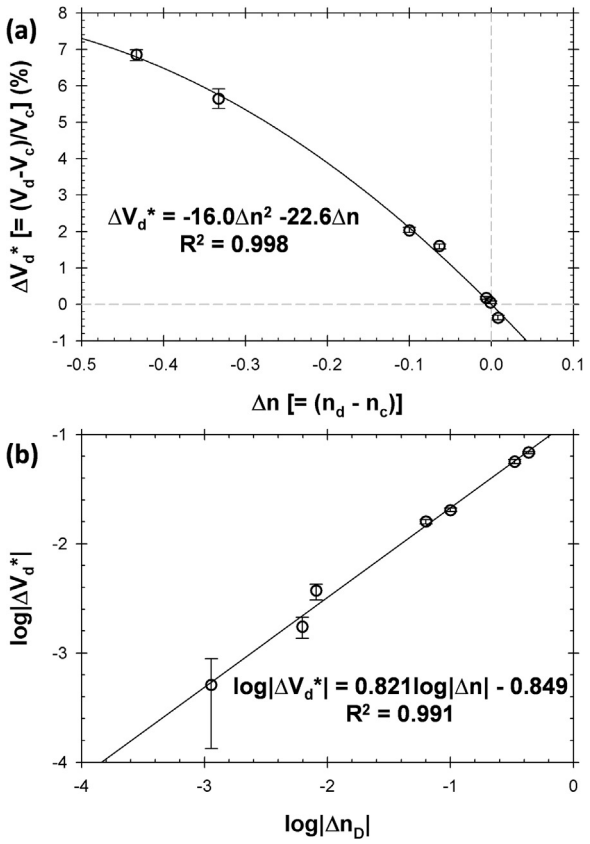

Fig. 4. (a) Relationship between ΔV_d^* and Δn ($= n_d - n_c$). The error bar represents the variation of thirty consecutive periods of the electric signal. (b) Logarithmic scale plot of $|\Delta V_d^*|$ versus $|\Delta n|$.

driven setup (in ESI S.4), and it demonstrates the great potential for the simplification of two-phase flow generation in the microfluidic systems with higher mobility but less cost.

3.2. Instantaneous size and velocity measurement of bubbles/droplets

To measure the instantaneous size and velocity of the fluid segments of dispersed phase fluid inside the microfluidic channel, distilled water – air flow was used as the example and generated with constant pressure sources by two pressure regulators. There are three characteristic flow types, i.e., pure liquid flow, slug flow, and annular flow [40], and its flow map is shown in Fig. S5 in ESI. In this work, only the signal in the slug flow regime would be considered for the bubble size and velocity analysis.

Fig. 5(a) shows the signals of distilled water – air flow passing through the dual optical microfiber system, where Δt is the travel time for a bubble passing two microfibers. The mean velocity of the dispersed segment (here is the bubble) v_d is determined as

$$v_d = \frac{L}{\Delta t} \quad , (1)$$

and the size of the dispersed segment l_d is

$$l_d = v_d \times T_d \quad , (2)$$

where L is the distance between two optical microfibers, Δt and T_d are the contact period with a microfiber and the travelling time between two microfibers of any specific test sample, as shown in Fig. 5(a), respectively.

The l_d and v_d measurements by direct image analysis (in ESI S.6) and by the present optical microfibers are compared in Fig. 5(b–(c), where subindex img and f represent measurements from image analysis and from optical fiber method, respectively. It shows excellent agreement in wide segment size and velocity ranges of 1.03-5.05 mm and 1.94-71.5 mm/s, respectively. Both the rise and fall response time of the fiber signal are less than 10 ms in case of v_d = 71.5 mm/s, which implies that this system could at least detect 50 samples per second. The uncertainties for the on-line velocity and size measurements of micro-two-phase flow are lower than 0.4% and 3.4%, respectively. The detailed analysis is described in ESI S.7.

It is important to note that the real-time size and velocity measurement of bubble can be easily achieved by the optical system integrating with a LabVIEW-coded program in this work; however, the on-line direct image analysis is still not possible due to long waiting time for the download of recorded images from high speed camera for further analysis. The present microfiber on-line detecting method with simple, low-cost and robust advantages is significantly superior to those by image analysis in most applications. Besides, the maximum deviation measured by both methods was less than 3%, which means that this newly developed optical microfiber chip is a reliable sensing technique for real-time bubble/droplet size and velocity measurements for various microfluidic applications.

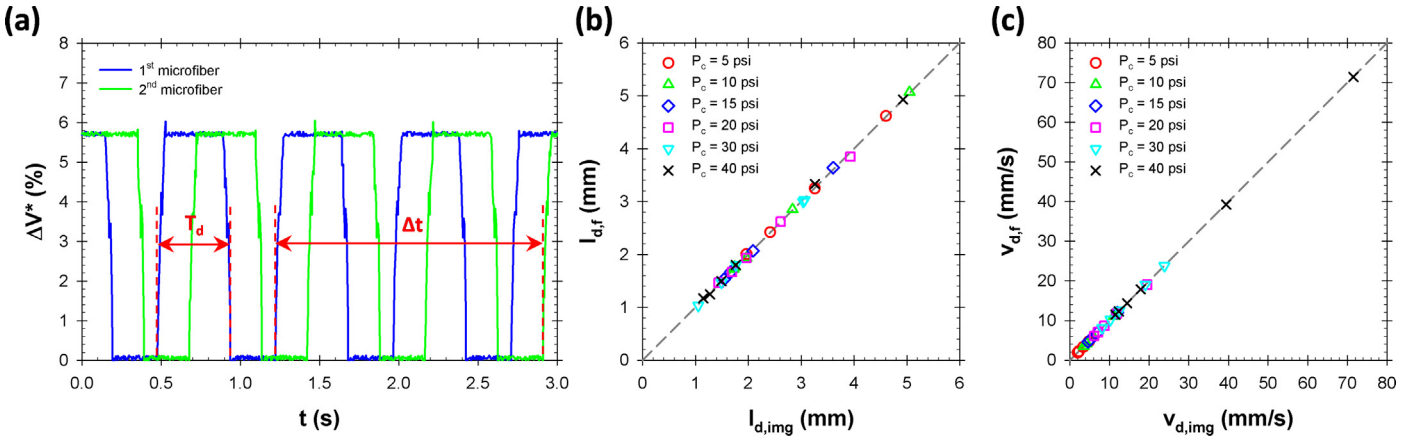

Fig. 5. (a) Normalized microfiber signals of distilled water – air flow passing through the dual microfiber system. Comparison of the (b) length l_d and (c) velocity v_d of dispersed segments measured by the microfiber and image analysis methods. Each data indicates the average of ten measurements. P_c is the pumping pressure in the upstream of the main channel (please see also in ESI S.5).

Table 1
Measurements of refractive index, length, and velocity of a series of different tiny droplets.

N	C_{gly} (%)	$\Delta V_d{}^*$ (%)	n_d	$n_{d,f}$	ε_n (%)	$l_{d,img}$ (μm)	$l_{d,f}$ (μm)	ε_l (%)	$v_{d,img}$ (mm/s)	$v_{d,f}$ (mm/s)	ε_v (%)
1	70	0.231	1.4273	1.4265	−0.057	897	904	0.74	1.847	1.849	0.11
2	0	2.06	1.3341	1.3396	0.42	903	905	0.19	1.880	1.848	−1.7
3	80	−0.250	1.4416	1.4402	−0.10	898	886	−1.3	1.832	1.847	0.87
4	30	1.56	1.3697	1.3666	−0.22	907	893	−1.5	1.845	1.848	0.14
5	95	−100	1.4644	[a]	[a]	901	893	−0.85	1.864	1.848	−0.88
6	73	0.0716	1.4320	1.4314	−0.040	[b]	903	[b]	[b]	1.848	[b]

[a] The refractive index of the droplet could not be measured since the refractive index of 95% aqueous glycerol solution is higher than that of the optical microfiber.
[b] The droplet size and droplet velocity could not be measured by direct image analysis with microscope due to the indistinguishable interface of the Hexadecane and 73% aqueous glycerol solution.

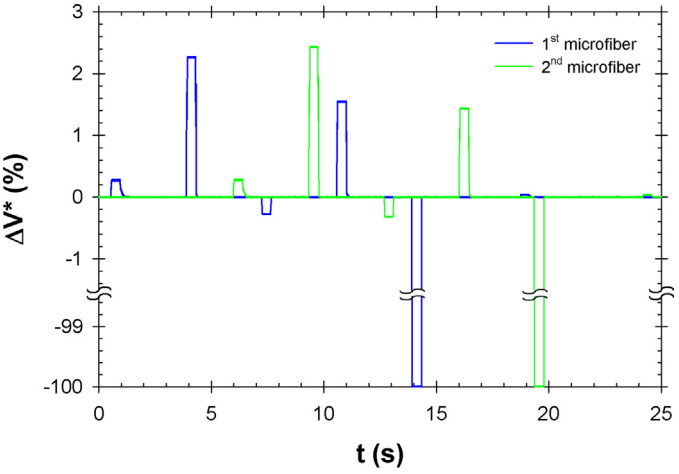

Fig. 6. Detected signals of a series of different fluid samples passing through two optical microfibers in the microfluidic chip with constant flow rate 1 ml/h.

3.3. On-line refractive index, size, and velocity measurement of a series of tiny droplets

To reduce the consumption of costly biochemical samples in such as screening applications, we demonstrate the on-line simultaneous refractive index, sample size and velocity measurements of tiny droplets by this novel optical microfiber system. Six tiny aqueous droplets (~100 nL) with different glycerol concentrations in random concentration order were carried by Hexadecane to pass through the microfibers with the flow rate of 1 ml/h. The test results are listed in Table 1, and the detected signals of two microfibers are shown in Fig. 6. In Table 1, N indicates the test sequence, ε represents the measuring error and the subindex n, l and v are the measuring quantities. The n_d value was obtained by summing up n_c (here is Hexadecane) and Δn calculated from the measured $\Delta V_d{}^*$ based on the regression equation in Fig. 4(b). The maximum measuring error of refractive index (ε_n) was below 0.5% among all tests. Furthermore, the measuring errors of sample size (ε_l) and sample velocity (ε_v) between the optical sensor system and image analysis were less than 2%. It demonstrates that the present system could accurately perform a series of on-line measurements of refractive index, sample size, and sample velocity at the same time for tiny sample volume of around 100 nL (or further reduced till 100 pL by simply scale down the channel dimensions to 1/10).

3.4. Concentration measurement

Since the concentration detection is important in many chemical and analytical applications, this optical microfiber system was then tested for concentration measurements of 17 different droplet-based aqueous glycerol solutions. The refractive index and concentration relation of aqueous glycerol solutions was obtained from the regression equation

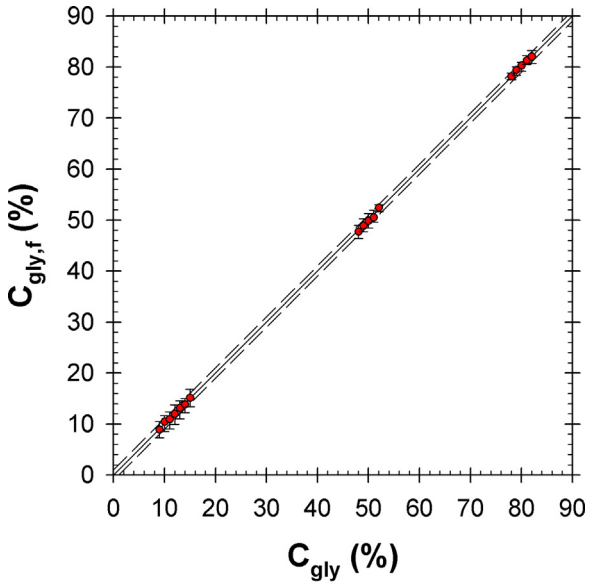

Fig. 7. Concentration measurement of droplet-based aqueous glycerol solutions, where $C_{gly,f}$ is the concentration measured by the optical microfiber system. The error bars represent the deviations of ten measurements. The dashed lines indicate the ±1% −deviation band of $C_{gly,f} = C_{gly}$.

($n = 2.0479 \times 10^{-2} C_{gly}{}^2 + 1.2146 \times 10^{-1} C_{gly} + 1.3325$) from Hoyt [39] (as shown in ESI Fig. S2), and the test samples with different glycerol concentrations were carried by Hexadecane for optical microfiber measurements. Fig. 7 shows the detecting results, where C_{gly} and $C_{gly,f}$ are the given concentration and the measured value from the microfiber, respectively. Each data represents the average of ten tests, and the corresponding error bar indicates the deviations of the measurements. The dashed lines illustrate the ±1%-deviation band of $C_{gly,f} = C_{gly}$. It shows clearly that this optical microfiber system can be accurately used for the concentration measurement in wide range of aqueous glycerol solutions within ±1%-deviation as shown in Fig. 7, i.e., the accuracy of concentration measurement is about 1%. The concentration resolution of this optical detecting system is estimated to be 0.2% by differentiating the n-Cgly regression equation (as shown in ESI Fig. S2) with respect to n based on the refractive index resolution of 2×10^{-4}.

4. Conclusions

In this work, we provided a high-throughput, simple and sensitive technique with high resolution and precision but low cost for measuring the refractive index of bubble/droplet two-phase flows with the need of only tiny sample volume (about 100 nL or less) in a novel microfluidic system integrated with optical microfibers. The long-time existing low space resolution problem of immersed optical microfiber in the microfluidic channel has been successfully solved by the crossflow of microfiber and a special “soft sealing”

Table 2
Comparison of detection techniques in bubble/droplet-based microfluidic systems.

Method	Sensitivity	Space resolution	On-line analysis throughput	Cost	Measured parameters	Note
Bright-Field Microscopy	Low	High	Low/Fair[a]	Fair	Size [10–13], velocity [11], concentration [12], segment morphology [13]	Intuitive, simple
Fluorescence Microscopy	High	High	Low	Fair	Concentration [14–17]	Intuitive, labelling required
Optical Absorption	Low	Low	Fair	Low	Size [18,21], frequency [18], concentration [18–21]	High positioning required
Electrochemical Detection	Fair	Fair	High	Fair	Size [25,26], velocity [25,26], frequency [26], concentration [28]	Sensor embedded, microlithography required
Laser-Induced Fluorescence	Ultra-high	High	High	Expensive	Concentration [29–33]	Labelling required
Raman Spectroscopy	High	High	Fair	Very expensive	Concentration [34–38]	Multiple analysis
Optical Evanescent Field	High	Low–Fair	Fair	Low	Refractive index [39], size [21], concentration [40–42]	Sensor embedded
Present Work	High	High	High	Low	Refractive index, size, velocity, concentration, frequency	Simple, sensor embedded

[a] On-line analysis throughput gets higher once the detection system is integrated with a line scan camera.

design in the microfluidic channel. It brings the above-mentioned advantages but without tedious efforts for position calibration and also for preventing leakage during operation. Different refractive index combinations of the microfiber n_f, continuous phase fluid n_c, and dispersed phase fluid n_d were studied. It is systematically analyzed and concluded that there are two operation modes in this optical microfiber sensing technique. For $n_d/n_f \geq 1$, the square-wave-like signal has high level of signal V_c and low level of zero, which has the highest signal visibility for a given continuous fluid n_c and is especially suitable for droplet sample counting or sorting purpose. As for $n_d/n_f < 1$, it is the necessary condition of refractive index measurements for different fluid samples, and their n_d values could be easily derived from the summation of Δn (calculated from the measured alternative voltage $\Delta V_d{}^*$ of the microfiber signal) and n_c. The detecting resolution Δn of this optical sensor system was estimated to be 2×10^{-4}, and accurate on-line concentration measurement could be also achieved with about 0.2% resolution. This method offers great potential for applications such as on-line high-throughput screening or biochemical reaction monitoring. Furthermore, by using dual optical microfibers, the functions of this sensing system have been further extended to measure the bubble size and velocity in real-time with excellent agreement (less than 3% deviation) in comparison with that by image analysis. The overall measurement uncertainty was analyzed to be no more than 3.4%, and high-throughput on-line detecting speed up to 50 samples per second has been easily obtained. As a concluding remark, the brief performance comparison between different bubble/droplet detection techniques and this work has been summarized in Table 2.

Acknowledgement

We acknowledge the financial support from Ministry of Science and Technology, Taiwan under contract number MOST 102-2221-E-002-081-MY3.

Appendix A. Supplementary data

Supplementary data associated with this article can be found, in the online version, at http://dx.doi.org/10.1016/j.snb.2016.07.027.

References

[1] X. Niu, F. Gielen, J.B. Edel, A.J. deMello, A microdroplet dilutor for high-throughput screening, Nat. Chem. 3 (2011) 437–442.
[2] A. Sciambi, A.R. Abate, Accurate microfluidic sorting of droplets at 30 kHz, Lab Chip 15 (2015) 47–51.
[3] H. Yamaguchi, M. Maeki, K. Yamashita, H. Nakamura, M. Miyazaki, H. Maeda, Controlling one protein crystal growth by droplet-based microfluidic system, J. Biochem. 153 (2013) 339–346.
[4] X. Yu, G. Cheng, M.D. Zhou, S.Y. Zheng, On-demand one-step synthesis of monodisperse functional polymeric microspheres with droplet microfluidics, Langmuir 31 (2015) 3982–3992.
[5] M. Prakash, N. Gershenfeld, Microfluidic bubble logic, Science 315 (2007) 832–835.
[6] P. Garstecki, M.J. Fuerstman, H.A. Stone, G.M. Whitesides, Formation of droplets and bubbles in a microfluidic T-junction—scaling and mechanism of break-up, Lab Chip 6 (2006) 437–446.
[7] S. Jakiela, S. Makulska, P.M. Korczyk, P. Garstecki, Speed of flow of individual droplets in microfluidic channels as a function of the capillary number, volume of droplets and contrast of viscosities, Lab Chip 11 (2011) 3603–3608.
[8] K. Churski, P. Korczyk, P. Garstecki, High-throughput automated droplet microfluidic system for screening of reaction conditions, Lab Chip 10 (2010) 816–818.
[9] D.R. Link, S.L. Anna, D.A. Weitz, H.A. Stone, Geometrically mediated breakup of drops in microfluidic devices, Phys. Rev. Lett. 92 (2004) (pp. 054503).
[10] C.H.J. Schmitz, A.C. Rowat, S. Köster, D.A. Weitz, Dropspots: a picoliter array in a microfluidic device, Lab Chip 9 (2009) 44–49.
[11] J.E. Kreutz, L. Li, L.S. Roach, T. Hatakeyama, R.F. Ismagilov, Laterally mobile, functionalized self-assembled monolayers at the fluorous-aqueous interface in a plug-based microfluidic system: characterization and testing with membrane protein crystallization, J. Am. Chem. Soc. 131 (2009) 6042–6043.
[12] F. Shen, W. Du, J.E. Kreutz, A. Fok, R.F. Ismagilov, Digital PCR on a SlipChip, Lab Chip 10 (2010) 2666–2672.
[13] M.P.N. Bui, C.A. Li, K.N. Han, J. Choo, E.K. Lee, G.H. Seong, Enzyme kinetic measurements using a droplet-based microfluidic system with a concentration gradient, Anal. Chem. 83 (2011) 1603–1608.
[14] V. Trivedi, A. Doshi, G.K. Kurup, E. Ereifej, P.J. Vandevord, A.S. Basu, A modular approach for the generation, storage, mixing, and detection of droplet libraries for high throughput screening, Lab Chip 10 (2010) 2433–2442.
[15] S.R.T. Neil, C.M. Rushworth, C. Vallance, S.R. Mackenzie, Broadband cavity-enhanced absorption spectroscopy for real time, in situ spectral analysis of microfluidic droplets, Lab Chip 11 (2011) 3953–3955.
[16] K. Churski, T.S. Kaminski, S. Jakiela, W. Kamysz, W. Baranska-Rybak, D.B. Weibel, P. Garstecki, Rapid screening of antibiotic toxicity in an automated microdroplet system, Lab Chip 12 (2012) 1629–1637.
[17] J. Yue, F.H. Falke, J.C. Schouten, T.A. Nijhuis, Microreactors with integrated UV/Vis spectroscopic detection for online process analysis under segmented flow, Lab Chip 13 (2013) 4855–4863.
[18] W.Z. Song, X.M. Zhang, A.Q. Liu, C.S. Lim, P.H. Yap, H.M. Hosseini, Refractive index measurement of single living cells using on-chip Fabry-Pérot cavity, Appl. Phys. Lett. 89 (2006) (pp. 203901).
[19] W.Z. Song, A.Q. Liu, S. Swaminathan, C.S. Lim, P.H. Yap, T.C. Ayi, Determination of single living cell's dry/water mass using optofluidic chip, Appl. Phys. Lett. 91 (2007) (pp. 223902).
[20] X. Niu, M. Zhang, S. Peng, W. Wen, P. Sheng, Real-time detection, control, and sorting of microfluidic droplets, Biomicrofluidics 1 (2007) (pp. 044101).
[21] C. Elbuken, T. Glawdel, D. Chan, C.L. Ren, Detection of microdroplet size and speed using capacitive sensors, Sens. Actuators A Phys. 171 (2011) 55–62.
[22] S. Liu, Y. Gu, R.B.L. Roux, S.M. Matthews, D. Bratton, K. Yunus, A.C. Fisher, W.T.S. Huck, The electrochemical detection of droplets in microfluidic devices, Lab Chip 8 (2008) 1937–1942.
[23] X. Hu, X. Lin, Q. He, H. Chen, Electrochemical detection of droplet contents in polystyrene microfluidic chip with integrated micro film electrodes, J. Electroanal. Chem. 726 (2014) 7–14.
[24] S. Gu, Y. Lu, Y. Ding, L. Li, H. Song, J. Wang, Q. Wu, A droplet-based microfluidic electrochemical sensor using platinum-black microelectrode and

its application in high sensitive glucose sensing, Biosens. Bioelectron. 55 (2014) 106–112.
[25] D. Pekin, Y. Skhiri, J.C. Baret, D.L. Corre, L. Mazutis, C.B. Salem, F. Millot, A.E. Harrak, J.B. Hutchison, J.W. Larson, D.R. Link, P. Laurent-Puig, A.D. Griffiths, V. Taly, Quantitative and sensitive detection of rare mutations using droplet-based microfluidics, Lab Chip 11 (2011) 2156–2166.
[26] L. Mazutis, J. Gilbert, W.L. Ung, D.A. Weitz, A.D. Griffiths, J.A. Heyman, Single-cell analysis and sorting using droplet-based microfluidics, Nat. Protoc. 8 (2013) 870–891.
[27] S. Maillot, A. Carvalho, J.P. Vola, C. Boudier, Y. Mély, S. Haacke, J. Léonard, Out-of-equilibrium biomolecular interactions monitored by picosecond fluorescence in microfluidic droplets, Lab Chip 14 (2014) 1767–1774.
[28] B. Vazquez, N. Qureshi, L. Oropeza-Ramosb, L.F. Olguin, Effect of velocity on microdroplet fluorescence quantified by laser-induced fluorescence, Lab Chip 14 (2014) 3550–3555.
[29] J.W. Choi, G.J. Kim, S. Lee, J. Kim, A.J. deMello, S.I. Chang, A droplet-based fluorescence polarization immunoassay (dFPIA) platform for rapid and quantitative analysis of biomarkers, Biosens. Bioelectron. 67 (2015) 497–502.
[30] M.P. Cecchini, J. Hong, C. Lim, J. Choo, T. Albrecht, A.J. deMello, J.B. Edel, Ultrafast surface enhanced resonance Raman scattering detection in droplet-based microfluidic systems, Anal. Chem. 83 (2011) 3076–3081.
[31] S.K. Luther, S. Will, A. Braeuer, Phase-specific Raman spectroscopy for fast segmented microfluidic flows, Lab Chip 14 (2014) 2910–2913.
[32] L. Wu, Z. Wang, S. Zong, Y. Cui, Rapid and reproducible analysis of thiocyanate in real human serum and saliva using a droplet SERS-microfluidic chip, Biosens. Bioelectron. 62 (2014) 13–18.
[33] T.A. Meier, R.J. Beulig, E. Klinge, M. Fuss, S. Ohla, D. Belder, On-chip monitoring of chemical syntheses in microdroplets via surface-enhanced Raman spectroscopy, Chem. Commun. 51 (2015) 8588–8591.
[34] I.J. Hidi, M. Jahn, K. Weber, D. Cialla-May, J. Popp, Droplet based microfluidics: spectroscopic characterization of levofloxacin and its SERS detection, Phys. Chem. Chem. Phys. 17 (2015) 21236–21242.
[35] P. Polynkin, A. Polynkin, N. Peyghambarian, M. Mansuripur, Evanescent field-based optical fiber sensing device for measuring the refractive index of liquids in microfluidic channels, Opt. Lett. 30 (2005) 1273–1275.
[36] L. Zhang, P. Wang, Y. Xiao, H. Yu, L. Tong, Ultra-sensitive microfibre absorption detection in a microfluidic chip, Lab Chip 11 (2011) 3720–3724.
[37] K. Li, G. Liu, Y. Wu, P. Hao, W. Zhou, Z. Zhang, Gold nanoparticle amplified optical microfiber evanescent wave absorption biosensor for cancer biomarker detection in serum, Talanta 120 (2014) 419–424.
[38] Z. Li, Y. Xu, W. Fang, L. Tong, L. Zhang, Ultra-sensitive nanofiber fluorescence detection in a microfluidic chip, Sensors 15 (2015) 4890–4898.
[39] L.F. Hoyt, New table of the refractive index of pure glycerol at 20 °C, Ind. Eng. Chem. 26 (1934) 329–332.
[40] A.B. Wang, I.C. Lin, Y.W. Hsieh, W.P. Shih, G.W. Wu, Effective pressure and bubble generation in a microfluidic T-junction, Lab Chip 11 (2011) 3499–3507.

Biographies

Yu-Wen Hsieh received his B.S. degree in Department of Mechanical Engineering, National Taiwan University in 2008. He is a Ph.D. student in Institute of Applied Mechanics, National Taiwan University. His present research interests include applications of droplet microfluidics and patterned coating.

An-Bang Wang received the Dr.-Ing.-degree at the Institute of Fluid Mechanics, University of Erlangen-Nürnberg, Germany in 1991. He joined the Institute of Applied Mechanics, National Taiwan University and became a full professor in 2001. From 2002 to 2004, he served as the director of Optomechatronics Education Resource center, Ministry of Education, Taiwan, ROC. From 2004 to 2008, he served as the chairman of the display technology Education Program and counselor of advisory office, Ministry of Education, Taiwan, ROC. He has been honored with the 2013 Distinguished Engineering Professor Award granted by Chinese Institute of Engineers (CIE), Taiwan, ROC. Numerous students received best paper awards in various competitions under his supervision. His current research interests include advanced coating and 3D-printing technology, microfluidic platform for industrial applications, display and optomechatronic systems, and biomimetics.

Xuan-Yi Lu received his B.S. degree in Department of Electrical Engineering, National Tsing Hua University in 2013. He is a M.S. student in Graduate Institute of Photonics and Optoelectronics, National Taiwan University. His research topic is mainly focused on the applications of optical microfiber sensing.

Lon A. Wang received his Ph.D. degree in Optical Sciences Center from the University of Arizona in 1988. Following graduation, he continued as postdoctoral researcher. In 1989 he joined Bell Communication Research (BEELCORE) where he worked in the areas of wavelength division multiplexing technologies and optical fiber network system technologies. In 1992, he joined the Institute of Electro-Optical Engineering and the Department of Electrical Engineering, National Taiwan University, where he is currently a professor. His current interests are design, fabrication, and modeling of active and passive fiber devices and guided-wave components for photonic integrated circuits, optical fiber communication and sensing system applications; semiconductor nano-fabrication for integrated circuits and electro-optical devices.